American Journal of Earth Science and Engineering
2018; 1(3): 150-165
http://www.aascit.org/journal/ajese

AASCIT American Association for Science and Technology

Petrology of Kaersutite Megacryst-Bearing Benmoreites from the Tignere Volcanic Domain (Adamawa Plateau, Cameroon)

Isaac Bertrand Gbambié Mbowou[1, *], Nilson Francisquini Botelho[2], Ismaïla Ngounouno[1]

[1]Department of Mines and Geology, University of Ngaoundere, Meiganga, Cameroon
[2]Geosciences Institute, University of Brasilia (UnB) Asa Norte, Brasilia, Brazil

Email address

mbowou2000@yahoo.fr (I. B. G. Mbowou)
[*]Corresponding author

Citation

Isaac Bertrand Gbambié Mbowou, Nilson Francisquini Botelho, Ismaïla Ngounouno. Petrology of Kaersutite Megacryst-Bearing Benmoreites from the Tignere Volcanic Domain (Adamawa Plateau, Cameroon). *American Journal of Earth Science and Engineering.* Vol. 1, No. 3, 2018, pp. 150-165.

Received: February 15, 2018; **Accepted**: March 10, 2018; **Published**: April 27, 2018

Abstract: Kaersutite megacryst-bearing benmoreites from the Tignere volcanic domain belong to the Adamawa Plateau (Cameroon). These rocks are characterized by a porphyritic texture and consist of plagioclase, alkali feldspar, amphibole, clinopyroxene, biotite, Fe-Ti oxides and apatite phenocrysts with amphibole megacrysts. Benmoreites display negative P, Ti and Rb anomalies with relatively low $^{87}Sr/^{86}Sr$ ratios (0.7037). Kaersutite megacrysts (mg#: 0.67) and phenocrysts (mg#: 0.66) are relatively similar in composition and seem to be generated from the same magma and under similar thermobarometric conditions as evidenced by mineral chemistry. Benmoreites from Tignere are to be regarded as the product of fractional crystallization processes from basaltic lava.

Keywords: Benmoreite, Fractional Crystallization, Tignere Volcanic Domain, Adamawa Plateau

1. Introduction

The Tignere volcanic domain belongs to the Adamawa plateau, central Cameroon (Figure 1) it is a magmatic complex that has several volcanic domes and necks (e.g: Hossere Doro, Hossere Kangur, Hossere Libong, Djinga Tadorgal massif), surrounded by lava flows and granitoids. The studied benmoreites were sampled on the Djinga Tadorgal massif, which is located ~100 km at west of Ngaoundere and ~25 km to the northwest of Tignere. Benmoreites from Adamawa Plateau were previously described from the Tchabal Nganha volcano [1] and N and E of Ngaoundere [2]. Benmoreites from Djinga Tadorgal are part of the Tignere volcanic domain and are characterized by the occurrence of amphibole megacrysts. These rocks belong to an alkaline bimodal series [3], due to the sporadic presence of intermediate rocks. This "Daly Gap" feature would suggest that melts with intermediate compositions might form a transition layer between basaltic and silicic melts in zoned magma chambers ([4]; [5]). According to [6], the viscosity of such phenocryst- (and megacryst)-rich magmas is high, they are immobile and rarely reach the surface during eruptions. Nonetheless, corresponding rocks, mugearites and benmoreites, occur sometimes as lava flows. Such rocks are more common as enclaves in volcanic rocks of various compositions.

The amphibole megacrysts (~5 cm long) were reported within the Adamawa plateau basalts at the Tchabal Nganha volcano [1], and along the Cameroon Line in the gabbros from Kokoumi [7] and the basalts from Oku [8] (see Figure 1). Kaersutite megacrysts (3−8 cm) were described also in alkaline basalts of southern flank of Etna, Italy [9], Canary Islands [10]) and Mont Blanc, South Quebec ([11].

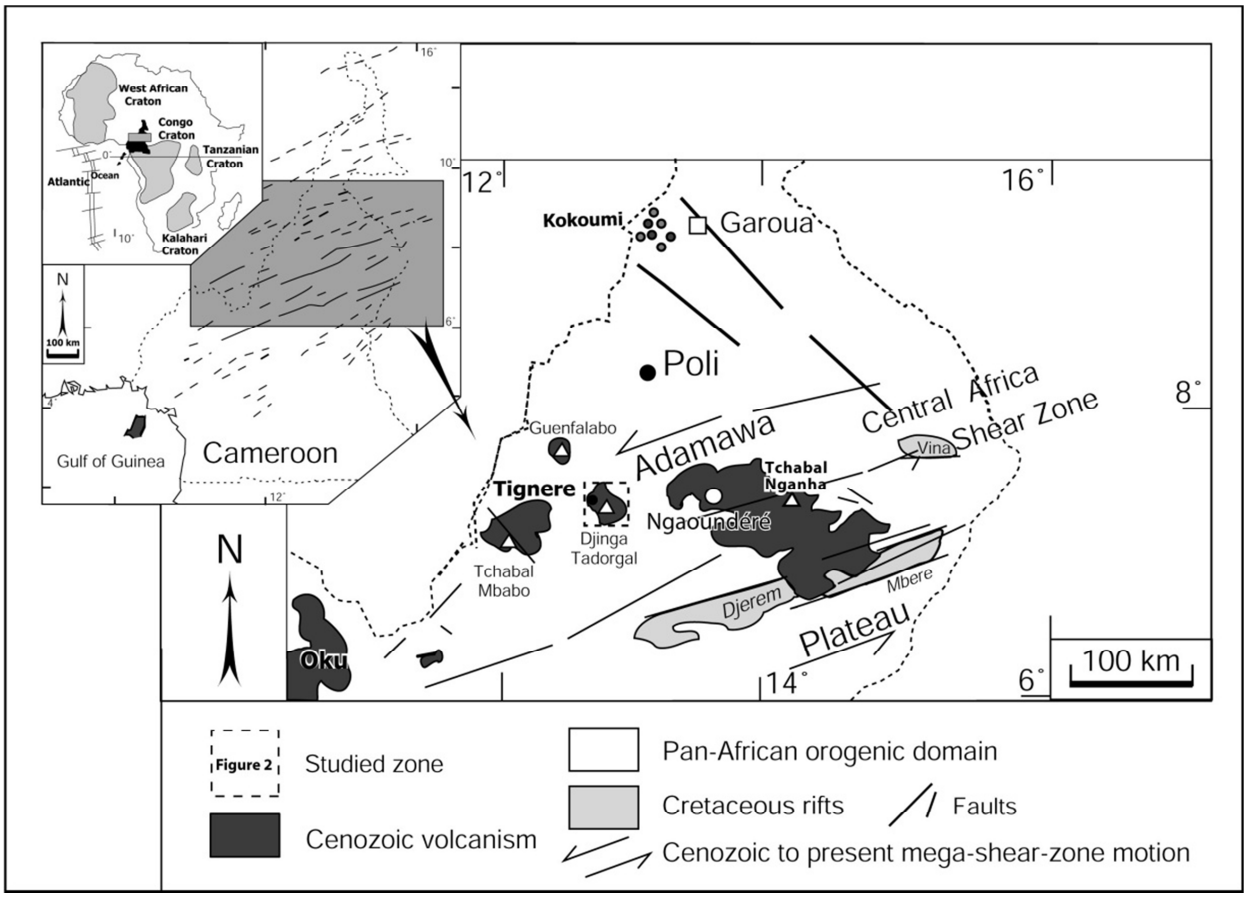

Figure 1. *Location of the studied zone in the Adamawa Plateau.*

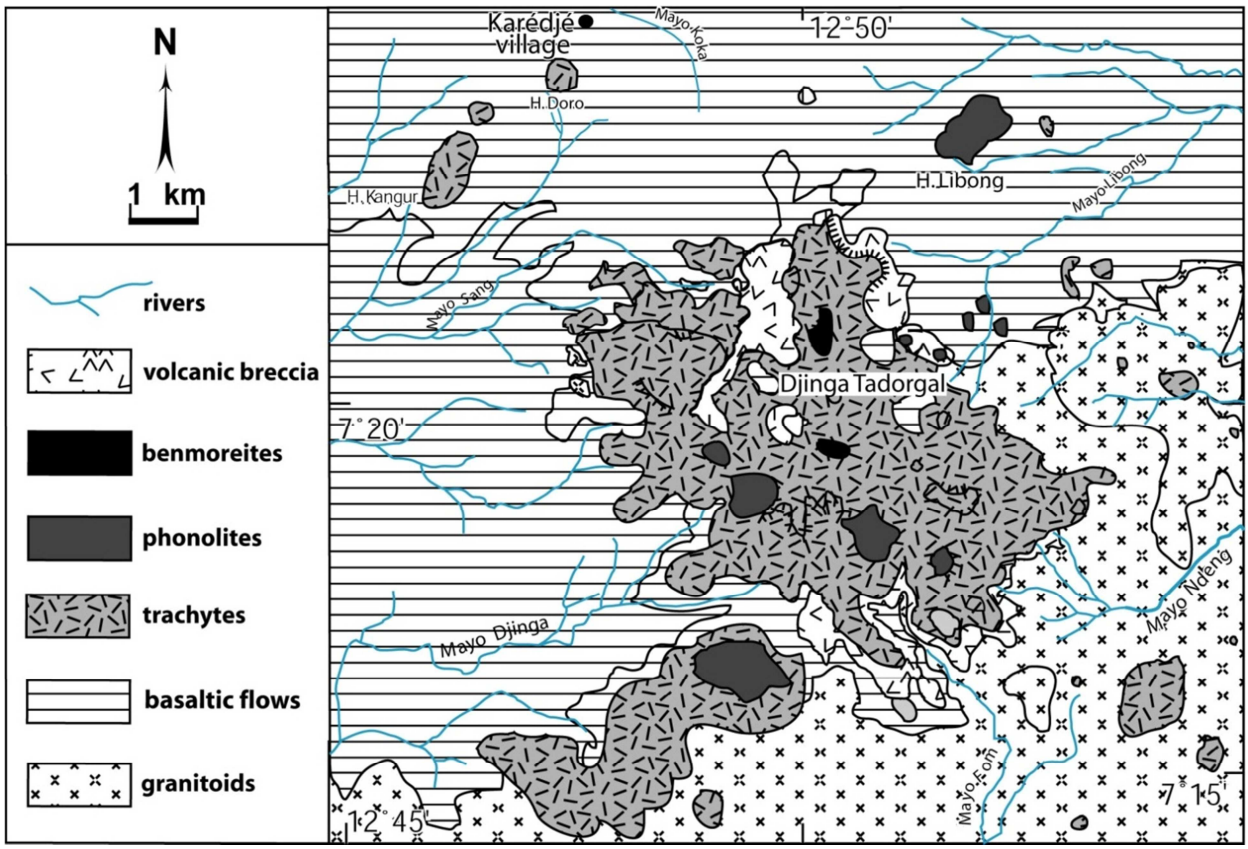

Figure 2. *Sketch of the geological map of the SE of Tignere volcanic domain (modified after [3]).*

In the Tignere volcanic domain, Djinga Tadorgal massif is the more huge and high (1747 m.a.s.l) volcano. The studied benmoreite (with kaersutite megacrysts) occurs on this massif associated with basalt, trachyte, phonolite and volcanic breccia (Figure 2). Indeed, the kaersutite megacrysts (up to 8 cm long) are exceptional in the benmoreite from the Adamawa Plateau. Thus, the study of kaersutite megacrysts-bearing benmoreites from Djinga Tadorgal Massif is an important source of information for the knowledge of their origin and the conditions of their genesis.

It is known that, benmoreites can occur from the fractional crystallization of trachybasaltic or alkali basaltic melts with or without crustal assimilation or by mixing of magmas of different compositions ([4]; [5]). The objective of this study is to present petrographic description of kaersutite megacrysts-bearing benmoreites from the Tignere volcanic domain, following by the results of the mineral chemistry and geochemical investigation. These data and modeling allowed the discussion of the most feasible models for the genesis of benmoreite melt during various stages of the volcanic evolution.

2. Geological Setting

The Adamawa Plateau belongs to the Pan-African fold belt of Central Africa [12]. It is a tectono-magmatic domain, bounded respectively to the North and South, by the Adamawa and Djerem-Mbéré (see Figure 1) faults (oriented N70˚E) [13]. The basement of this Plateau consisted of Paleo-Proterozoic granites and gneiss (2.1 Ga; [14], was partially destabilized by the Pan-African orogenesis ([15]; [16]) and intruded by several post-Pan-African granitoids and dolerite [17]. The Cenozoic basaltic, felsic and intermediate lavas of alkaline to peralkaline composition locally overlap the basement.

The rock flows, domes and necks were found on Djinga Tadorgal massif. The majority of eruptions produced on this asymmetrical stratovolcano are typically strombolian. Vents are often more or less opened fractures.

The rock flows are essentially basaltic and outcrop around the massif. Much more widespread, these rock flows are formed of blocks of all sizes. The basaltic blocks are sparse angular or rounded (5−50 cm) sometime slightly weathered and accumulated as small isolated volcanoes (diameter: ~ 500 m; height <30 m). Some basaltic fragments are almost completely weathered and converted into reddish ferralitic soils.

Successive eruptions of lava produced the overlapping domes and necks of trachytes, phonolites and benmoreites, that tower above the surrounding landscape or the rock flows. These volcanic *necks and domes* of trachyte and phonolite are locally covered by blocks and slabs, limited around the foothill by volcanic breccia. The domes have irregular slopes (30°−60°) and subcircular or elongated basis. The necks of needle-shaped lava have circular bases (diameter: ≈ 200 m) and more or less steep slopes (40°−85°). These formations are strongly prismatic and dismantled into blocks, disseminated in chaos on the soil. Rubble is abundant on the flanks and dry beds of streams. *The necks* (height <20 m) of intermediate lavas (benmoreite) which are the solid igneous core of a volcano left behind after the softer cone has been eroded, outcrop beside the trachyte on the top of Djinga Tadorgal massif. Some blocks (0.3m to 1m) of these intermediate lavas are dotted around the necks.

The volcanic domes of Hossere Kangur, Hossere Doro and Hossere Libong (altitude: < 1600 m a.s.l), are disseminated to the northwest and to the northeast of the Djinga Tadorgal massif (altitude: 1747 m a.s.l). The edges of these domes are bounded by small steep cliffs (20−40 m high) and the lava blocks are accumulated to the foothill. The volcanic breccia more or less well stratified, covers the beds of some streams surrounding the Djinga Tadorgal massif. The granitoid outcrops are almost present on the whole southern and eastern sector (see figure 2). These outcrops are more or less altered and strongly fragmented into angular or rounded blocks of centimeter to metric size.

3. Methods

The mineral phases were analyzed in polished thin sections with the electron microprobe analyzer using a Cameca microprobe SX100 at the “Université Pierre et Marie Curie”, Paris VI (France). The standards data used for analysis are from natural (Si, Al and K on orthoclase, Ca on anorthite, Na on albite, P on apatite, Zr on zircon) and synthetic (Fe on Fe_2O_3, Ba on BaO_4, Sr on $SrSiO_3$) phases.

The measurements were carried out with a beam size of 10-100 μm, under the following conditions expressed in kV (accelerating voltage), nA (beam current) and s (counting times at the peak): Olivine (15 kV, 40 nA, 20 s for all elements, except Si (10 s)), clinopyroxene (15 kV, 40 nA, 20 s for Si, Al, Fe, Mg, Ca, Na, Mn and 30 s for Ti and Zr), amphibole (15 kV, 10 nA, 15 s for Si, Al, Mg, Na and K, 20 s for Ca and Ti, 25 s for Fe and Mn, 30 s for Cl and F), feldspar (15 kV, 10 nA, 5 s for all elements), Fe-Ti oxides (15 kV, 40 nA, 40 s for Ti, Fe, Mn, Mg, 10 s for Si, 15 s for Cr and 30 s for Al), rhönite (15 kV, 40 nA, 10 s for Si et Fe, 15 s for Ca and 20 s for all others elements), mica (15 kV, 10 nA, 20 s for K, Ti, Cl, Ca, Mg, Al, Si, 15 s for Fe, 30 s for Ba, Mn, Ni, F and Na), apatite (15 kV, 30 nA, 10 s for Ca and P, 15 s for F and Cl, 20 s for all others elements) and titanite (15 kv, 10 nA, 10 s for all elements). Measurements correction was carried out using the "PAP" program [18]. For geochemical analyses the samples were crushed in an agate shatterbox. Chemical whole-rock analyzes (lavas and amphibole megacryst) were carried out at the CRPG laboratory, Nancy. Major Elements were analyzed by ICP-AES and trace elements by ICP-MS. The rock samples were previously selected in order to limit superficial contamination, then crushed. For amphibole chemical analysis, megacrysts were separated from the host rock with a hammer then selected under binocular lens and crushed. Details of

analytical processes for samples were presented elsewhere [19].

Sample for Rb–Sr isotopic analyses were dissolved in mixed HF–HNO_3 (10:1) acid mixture; chemical separation was carried out by cation exchange chromatography; blanks were <1 ng. Sr isotopic ratios were measured on a VG Sector 54 multicollector thermal ionization mass spectrometer (TIMS) at the "Université Libre de Bruxelles" (Belgium).

4. Results

4.1. Petrography

4.1.1. Basanite

Basanite is characterized by a porphyritic texture, consists of olivine (1−2 mm), clinopyroxene (2.2−3.1 mm) and Fe-Ti oxides (0.5−0.6 mm) phenocrysts in a groundmass of clinopyroxene, Fe-Ti oxides and plagioclase microlites. Some phenocrysts of amphibole and biotite are also present as well as the rare rhönite crystals. Clinopyroxene phenocrysts are euhedral and twinned. Olivine phenocrysts are subhedral, cracked and their edges are sometimes destabilized into iddingsite. Some amphibole crystals are converted into Fe-Ti oxides, rhönite and biotite. The small dark red rhönite crystals are surrounded by Fe-Ti oxides.

4.1.2. Benmoreite

Amphibole megacrysts-bearing benmoreites are porphyritic, with phenocrysts of plagioclase (6−8 mm), alkali feldspar (2−5 mm), amphibole, clinopyroxene, biotite, Fe-Ti oxides (~1.2 mm) and apatite (0.5−0.9 mm), in a groundmass of alkali feldspar, clinopyroxene, amphibole and Fe-Ti oxides microlites. Feldspar phenocrysts are fractured and destabilized. Amphibole phenocrysts (1.3−2.1 mm) and megacrysts (6−8 cm) are dark-brownish with more or less destabilized rim (Figure 3). The majority of amphibole is optically homogeneous and unzoned. The amphibole megacrysts and biotite phenocrysts are euhedral to subhedral and contain apatite inclusions. Clinopyroxene phenocrysts (~ 2.5 mm) are green, euhedral and contain inclusions of Fe-Ti oxides and plagioclase.

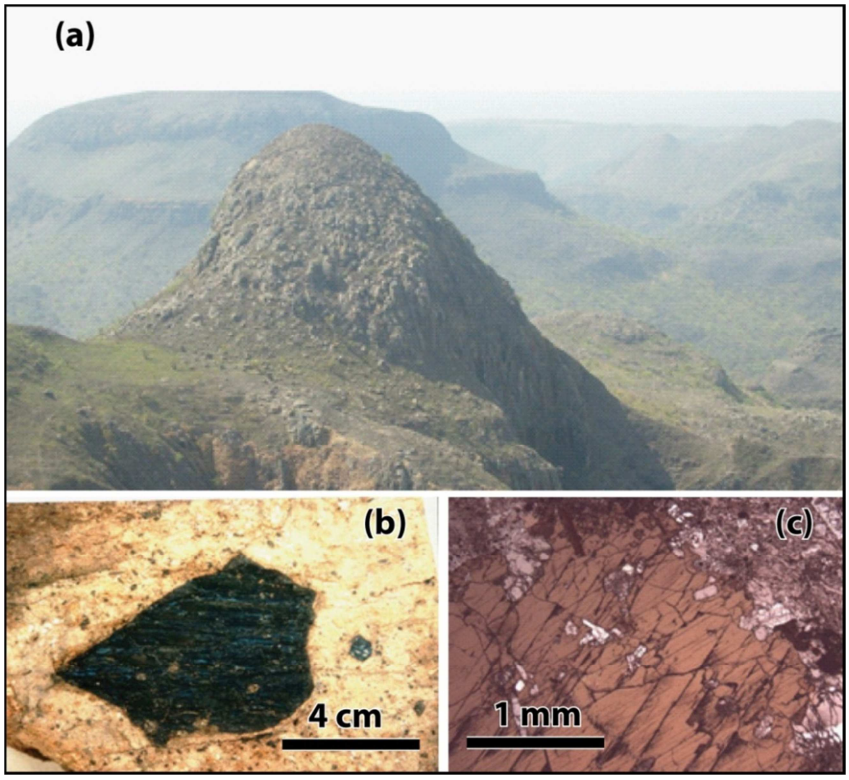

Figure 3. *(a) neck of benmoreite surrounded by trachytic outcrop (b) kaersutite megacryst (naked eye) in a benmoreite sample (c) microscopic aspect in thin section.*

4.1.3. Trachyte

Alkali feldspar (1−2 mm), clinopyroxene (0.5−1.5 mm), amphibole (0.6−1.2 mm), biotite, Fe-Ti oxides, apatite and titanite phenocrysts are scattered in the groundmass consisting of clinopyroxene, amphibole, alkali feldspar and Fe-Ti oxides microlites. Alkali feldspar phenocrysts are surrounded by Fe-Ti oxides microlites. Clinopyroxene and amphibole phenocrysts are scarce and highly destabilized into Fe-Ti oxides.

4.2. Geochemistry

4.2.1. Mineral Chemistry

i) Olivine

Forsterite (Fo) values, calculated for the analyzed olivine phenocrysts of the basanite (Table 1) reach 72−82 and 69−74, respectively for the core and the rim. The CaO contents are high (rim: ~ 0.41wt.% and core: ~ 0.43wt.%). The

crystallization temperatures for the core and the rim are respectively 1224 ± 60 °C and 1166 ± 48 °C (estimated after [20]) using bulk-rock composition as a liquid at the total pressure of 1 atm.

Table 1. *Representative chemical compositions and structural formula (on basis of 4 oxygens and 3 cations) of olivine (ph: phenocryst; c: core; r: rim).*

lavas-types	**basanite**					
sample nb.	**127**	**127**	**127**	**127**	**127**	**127**
description	**phc**	**ph.c**	**ph.r**	**ph.c**	**ph.r**	**ph.c**
SiO_2 (wt.%)	37.95	38.28	37.54	39.28	38.49	40.38
Al_2O_3	0.04	0.04	0.05	0.07	0.04	0.05
FeO	24.49	23.88	26.57	20.58	23.10	16.65
MnO	0.47	0.51	0.60	0.22	0.40	0.23
MgO	35.63	36.51	33.97	39.74	37.40	42.88
CaO	0.43	0.37	0.41	0.21	0.30	0.31
Total	99.16	99.75	99.40	100.10	99.75	100.55
Si (apfu)	1.012	1.011	1.011	1.014	1.010	1.019
Al	0.001	0.001	0.002	0.002	0.001	0.002
Fe^{2+}	0.546	0.527	0.598	0.444	0.507	0.352
Mn	0.011	0.011	0.014	0.005	0.009	0.005
Mg	1.417	1.438	1.364	1.529	1.464	1.614
Ca	0.012	0.010	0.012	0.006	0.009	0.008
Fo (%)	72.17	73.16	69.51	77.49	74.27	82.12
Fa	27.83	26.84	30.49	22.51	25.73	17.88

ii) Clinopyroxene

The clinopyroxene of basanite is either diopside or augite (according to the nomenclature of [21]; Figure 4). Some phenocrysts of augite and diopside (Table 2) are titaniferous (TiO_2: ~ 8.1wt.%; Ti: ~ 0.23 apfu: atom per formula unit) and Al-rich (Al_2O_3: ~ 12.4 wt.%; Al: ~ 0.55 apfu). The high contents of Ti and Al^{iv} in diopside and augite are linked to a low-pressure of crystallization [22].

The benmoreites contain also diopside (See Table 2) with TiO_2 contents reaching 2.19 wt.%. In the trachyte, the diopside ($Wo_{47}En_{41}Fs_{12}$ and $Wo_{50}En_{44}Fs_6$), are less titaniferous (TiO_2: 1.3−2.9 wt.%) than those from basalts.

The clinopyroxene of the studied basanite has elevated Al^{IV} values compared to those of the trachyte (see Table 2). In basanite, clinopyroxene has sufficient Al to compensate the Si^{4+} deficiency in the tetrahedral site (T-site); low Al^{IV} contents displayed in the pyroxenes of trachyte are compensated by the substitution of Si by Fe^{3+} and/or Ti ([23].

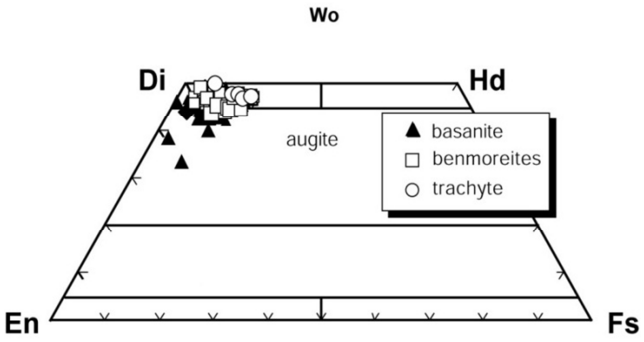

Figure 4. *Classification of clinopyroxene from the studied rocks in the Wo–En–Fs ternary diagram [21].*

Table 2. *Representative chemical compositions and structural formula (on the basis of 6 oxygens and 4 cations) of clinopyroxene (ph: phenocryst; c: core; r: rim; mc microcryst).*

lava-types	**basanite**							**benmoreite**				**trachyte**		
sample nb.	**127**	**127**	**127**	**127**	**127**	**127**	**127**	**207**	**206**	**293**	**293**	**293**	**293**	**293**
description	**ph.c**	**ph.c**	**ph**	**ph**	**ph.r**	**ph.c**	**mc**	**ph.r**	**ph.c**	**ph**	**ph**	**ph**	**ph.r**	**ph.c**
SiO_2 (wt.%)	45.59	47.20	47.30	37.04	45.96	48.17	49.28	46.91	47.73	50.14	48.86	49.92	48.84	48.10
TiO_2	4.56	3.27	3.51	8.14	2.80	2.13	1.27	2.03	2.19	1.76	2.89	2.85	1.30	1.49
Al_2O_3	8.27	6.93	6.41	12.46	8.39	7.17	4.57	6.44	5.71	2.62	3.38	2.35	3.92	3.81
FeO	6.09	5.68	6.01	10.73	6.28	7.23	5.66	9.57	7.89	8.71	9.49	8.77	9.09	8.95
MnO	0.10	0.07	0.17	0.07	0.09	0.15	0.07	0.51	0.27	0.77	1.20	0.83	0.61	0.60
MgO	12.17	13.11	12.71	11.16	13.37	13.25	15.63	11.06	12.82	11.99	11.14	12.08	11.93	11.88
CaO	23.49	23.56	23.89	19.38	22.60	22.03	22.20	21.63	22.95	20.59	20.53	20.93	22.28	22.45
Na_2O	0.67	0.72	0.74	0.95	0.58	0.77	0.60	1.13	0.88	1.75	1.85	1.06	1.28	1.16
Total	100.93	100.55	100.74	99.92	100.06	100.90	99.27	99.27	100.45	98.34	99.34	98.80	99.39	98.59
Fe_2O_3 (calc.)	2.76	3.63	3.52	9.22	4.87	3.66	4.16	5.38	6.07	4.22	4.87	2.76	6.51	6.69
FeO (calc.)	3.61	2.42	2.85	2.44	1.90	3.94	0.92	4.73	2.43	4.91	5.10	6.29	3.23	2.93
Total (calc.)	101.21	100.91	101.10	100.85	100.55	101.27	98.69	99.81	101.05	98.76	99.82	99.08	100.04	99.26
Si (apfu)	1.680	1.735	1.742	1.396	1.694	1.764	1.828	1.764	1.762	1.895	1.841	1.921	1.830	1.819
Ti	0.126	0.090	0.097	0.231	0.078	0.059	0.035	0.057	0.061	0.050	0.082	0.025	0.037	0.042
Al^{VI}	0.039	0.035	0.020	0.000	0.058	0.073	0.028	0.050	0.011	0.012	0.000	0.028	0.003	0.000
Al^{IV}	0.320	0.265	0.258	0.553	0.306	0.236	0.172	0.236	0.238	0.105	0.150	0.079	0.170	0.170
$Fe^{3+(VI)}$	0.076	0.100	0.098	0.261	0.135	0.101	0.116	0.152	0.169	0.120	0.138	0.080	0.184	0.179
Fe^{2+}	0.111	0.074	0.088	0.077	0.059	0.121	0.029	0.149	0.075	0.155	0.161	0.202	0.101	0.093
Mn	0.003	0.002	0.005	0.002	0.003	0.005	0.002	0.016	0.008	0.025	0.038	0.027	0.019	0.019

lava-types	basanite							benmoreite				trachyte		
sample nb.	127	127	127	127	127	127	127	207	206	293	293	293	293	293
description	ph.c	ph.c	ph	ph	ph.r	ph.c	mc	ph.r	ph.c	ph	ph	ph	ph.r	ph.c
Mg	0.669	0.719	0.698	0.627	0.734	0.723	0.864	0.620	0.706	0.676	0.626	0.693	0.666	0.670
Ca	0.927	0.928	0.942	0.783	0.892	0.864	0.883	0.872	0.908	0.834	0.829	0.863	0.894	0.910
Na	0.048	0.051	0.053	0.069	0.042	0.055	0.043	0.082	0.063	0.128	0.135	0.079	0.093	0.085
Wo (%)	48.60	49.03	50.04	38.31	46.19	45.02	45.96	47.43	48.91	47.62	47.61	46.63	49.93	50.55
En	44.47	46.92	45.02	58.98	51.35	47.77	53.40	43.39	47.80	42.60	41.72	41.32	44.80	44.99
Fs	6.93	4.05	4.94	2.71	2.46	7.21	0.63	9.18	3.29	9.78	10.67	12.05	5.27	4.45
Ti/Al	0.35	0.30	0.35	0.42	0.21	0.19	0.18	0.20	0.24	0.43	0.55	0.23	0.21	0.25

iii) Rhönite

The rhönite crystals (Table 3, Figure 5) are rich in CaO (9.6−11.8 wt.%), TiO_2 (10.3−12.2 wt.%) and MgO (11.5−13.3 wt.%) with low NaO contents (1.3−1.9 wt.%; Na < 0.6 apfu). Experimental work [24] indicates that the stability of the rhönite is limited to the pressures up to 0.06 GPa for temperatures calibrated between 840 °C and 1200 °C.

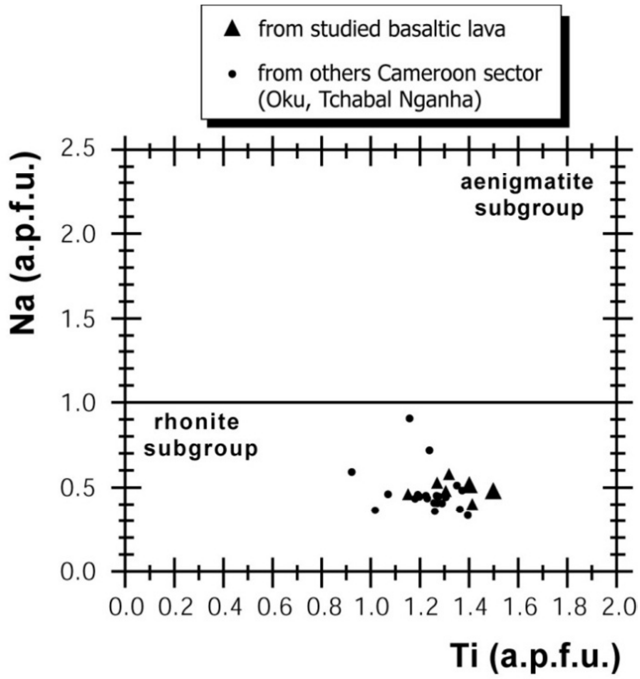

Figure 5. *Compositions of the studied rhönite are represented in comparison to those of the other Cameroon sector.*

Table 3. *Representative chemical compositions and structural formula (on the basis of 20 oxygens and 14 cations) of rhönite.*

lava-types	basanite				
sample nb.	127	127	127	127	127
SiO_2 (wt.%)	27.06	28.75	24.99	25.55	25.00
TiO_2	11.49	10.26	11.72	11.12	12.20
Al_2O_3	14.95	14.36	14.09	16.02	15.44
FeO	20.47	19.11	26.82	19.48	21.57
MnO	0.04	0.32	0.19	0.10	0.19
MgO	12.24	13.31	11.62	13.11	11.56
CaO	11.72	11.62	9.62	11.56	11.78
Na_2O	1.63	1.58	1.99	1.79	1.34
K_2O	0.05	0.07	0.17	0.02	0.01
Total	99.64	99.37	101.26	98.97	99.09
Fe_2O_3 (calc.)	4.56	4.80	10.77	6.57	6.36
FeO (calc.)	16.36	14.79	17.13	13.57	15.85
Total (calc.)	100.09	99.85	102.34	99.62	99.73
Si (apfu)	4.085	4.291	3.735	3.881	3.850
Ti	1.305	1.152	1.318	1.270	1.413
Al^{VI}	2.659	2.527	2.482	2.868	2.803
Al^{IV}	0.000	0.000	0.000	0.000	0.000
$Fe^{(3+)\,VI}$	0.518	0.539	1.211	0.751	0.737
Fe^{2+}	2.065	1.846	2.141	1.723	2.042
Mn	0.005	0.040	0.024	0.012	0.025

lava-types	**basanite**				
sample nb.	**127**	**127**	**127**	**127**	**127**
Mg	2.754	2.962	2.589	2.969	2.654
Ca	1.895	1.857	1.540	1.881	1.943
Na	0.477	0.458	0.577	0.526	0.399
K	0.009	0.012	0.032	0.004	0.002

iv) Mica

Phlogopite ($Fe^{2+}/(Fe^{2+}+Mg)$ <0.33; Al^{IV}: 2–3 apfu; Figure 6) analyzed in basanite contain F and TiO_2 respectively 3.3 wt.% and 9.2 wt.% (Table 4). The almost similar amount of F (~ 2.6 wt.%) and TiO_2 (~ 8.69 wt.%) are obtained for the phlogopite of benmoreite. Biotite phenocrysts were analyzed in benmoreite and trachyte (Table 4) with TiO_2 contents reaching 8.3 wt.%.

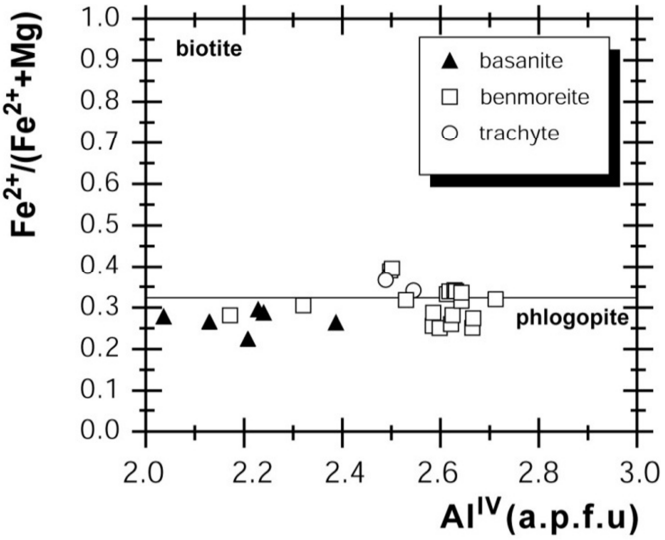

Figure 6. *Distribution of mica compositions in basalt, benmoreite and trachyte. Classification based on [25].*

Table 4. *Representative chemical compositions and structural formula (on the basis of 22 oxygens) of mica (ph: phenocryst; c: core).*

lava-types	**basanite**				**benmoreite**					**trachyte**	
sample nb.	**127**	**127**	**127**	**127**	**207**	**207**	**207**	**207**	**207**	**293**	**293**
description	**ph.c**	**ph.c**	**ph.c**	**ph.c**	**ph**	**ph**	**ph**	**ph**	**ph**	**ph**	**ph**
SiO_2 (wt.%)	36.65	38.98	37.91	36.50	36.73	36.90	36.34	36.75	37.12	37.35	37.32
TiO_2	9.17	8.32	8.69	8.11	8.48	8.56	8.20	8.50	8.37	7.64	5.97
Al_2O_3	12.79	12.00	13.61	11.86	14.92	14.45	14.42	14.31	14.58	14.20	14.21
FeO	11.35	9.24	9.79	9.42	9.74	10.03	10.75	10.89	13.35	13.20	14.41
MnO	0.12	0.10	0.00	0.10	0.05	0.00	0.16	0.09	0.31	0.55	0.65
MgO	15.19	13.44	15.33	13.09	16.26	16.01	15.96	15.57	14.42	14.29	13.95
CaO	0.50	8.60	0.05	7.88	0.07	0.06	0.07	0.00	0.02	0.00	0.09
Na2O	0.77	0.59	0.73	0.56	1.04	1.02	1.06	1.08	1.04	1.04	1.11
K2O	8.67	5.44	8.05	7.37	8.43	8.52	8.44	8.43	8.61	8.67	8.87
F	3.21	2.30	3.32	3.34	1.79	2.60	2.00	1.52	0.21	2.90	2.06
Cl					0.06	0.02	0.06	0.07	0.03	0.01	0.02
H_2O*	2.53	3.07	2.45	2.16	3.26	3.35	3.12	3.36	4.03	2.72	3.07
F as O	1.35	0.97	1.40	1.41	0.75	0.67	0.84	0.64	0.09	1.22	0.87
Cl as O	0.00	0.00	0.00	0.00	0.01	0.00	0.01	0.02	0.01	0.00	0.00
Total-(F+Cl)	96.56	97.69	95.57	96.30	96.47	97.22	96.25	96.28	97.91	98.16	97.45
Si (apfu)	5.421	5.612	5.491	5.047	5.335	5.378	5.334	5.376	5.371	5.455	5.512
Ti	1.019	0.901	0.972	0.977	0.927	0.938	0.905	0.935	0.910	0.839	0.663
Al^{IV}	2.229	2.036	2.387	2.240	2.665	2.622	2.666	2.624	2.629	2.545	2.488
Fe^{2+}	1.404	1.113	1.217	1.262	1.183	1.222	1.319	1.333	1.616	1.612	1.779
Mn	0.016	0.012		0.013	0.006	0.000	0.020	0.011	0.039	0.068	0.081
Mg	3.348	2.885	3.399	3.125	3.519	3.476	3.490	3.395	3.109	3.110	3.071
Ca	0.080	1.327	0.008	1.353	0.011	0.009	0.011	0.000	0.003	0.000	0.014
Na	0.222	0.166	0.212	0.174	0.292	0.288	0.302	0.307	0.291	0.294	0.318
K	1.635	0.999	1.528	1.507	1.562	1.585	1.580	1.572	1.589	1.616	1.672
F	1.504	1.049	1.565	1.695	0.823	0.736	0.931	0.705	0.098	1.341	0.963
Cl	0.000	0.000	0.000	0.000	0.015	0.004	0.014	0.017	0.008	0.002	0.005
OH	2.496	2.951	2.435	2.305	3.163	3.260	3.056	3.278	3.894	2.657	3.032
$Fe^{2+}/(Fe^{2+}+Mg)$	0.30	0.28	0.26	0.29	0.25	0.26	0.27	0.28	0.34	0.34	0.37

v) Oxides of Fe-Ti

The titano-magnetite is ubiquitous in the studied rocks (Table 5), with TiO_2 and FeO contents respectively 25.4 wt.% and 79.5 wt.%. TiO_2 contents are more higher in basanite (TiO_2: 23.1−25.4 wt.%) than in trachyte (TiO_2: 10.6−12.3 wt.%). In benmoreite TiO_2 values are more or less intermediate (TiO_2: 11.9−19.6 wt.%) between those of basanite and trachyte.

Table 5. *Representative chemical compositions and structural formula (on the basis of 32 oxygens) of Fe-Ti oxides.*

lava-types	basanite				benmoreite							trachyte		
sample nb.	**127**	**127**	**127**	**127**	**207**	**207**	**207**	**207**	**207**	**207**	**207**	**293**	**293**	**293**
SiO_2 (wt. %)	0.09	0.00	0.05	0.10	5.71	0.04	0.05	0.05	0.03	0.00	0.05	0.08	0.07	0.09
TiO_2	23.18	25.41	24.13	23.71	17.26	17.79	17.68	12.17	11.90	19.58	19.69	12.28	12.36	10.62
Al_2O_3	7.00	2.79	1.99	1.88	0.94	1.54	1.30	1.10	1.13	1.92	1.12	1.58	2.38	1.42
Cr_2O_3	0.00	0.00	0.00	0.00	0.00	0.03	0.01	0.02	0.00	0.00	0.02	0.06	0.09	0.04
FeO	61.13	63.14	67.55	66.54	59.16	70.61	69.65	78.69	79.06	70.69	72.25	79.39	78.40	79.52
MnO	0.55	0.70	0.79	0.66	0.92	1.53	1.66	3.47	3.48	2.05	2.40	2.85	1.88	2.62
MgO	5.60	3.97	2.64	3.00	9.89	4.19	3.97	1.26	1.32	3.00	1.76	1.87	2.47	1.70
CaO	0.03	0.12	0.10	0.52	0.24	0.11	0.26	0.05	0.00	0.06	0.24	0.03	0.06	0.02
Total	97.58	96.13	97.25	96.42	94.11	96.23	94.99	96.82	96.92	97.31	97.54	98.13	97.71	96.02
Ilmenite basis														
Fe_2O_3 (calc.)	31.99	32.95	35.62	35.93	39.22	46.40	45.88	49.42	49.95	42.61	42.86	52.78	51.69	53.64
FeO (calc.)	28.82	31.04	32.88	31.62	21.57	28.86	28.36	27.55	27.41	30.29	31.58	29.58	29.60	28.94
Total (calc.)	97.26	96.98	98.20	97.43	95.74	100.48	99.17	99.34	99.22	99.52	99.73	101.11	100.61	99.08
Ulvospinel basis														
Fe_2O_3 (calc.)	17.36	16.68	20.12	20.66	23.31	34.51	34.06	41.96	42.66	29.94	30.08	44.77	43.63	46.69
FeO (calc.)	41.98	45.68	46.83	45.36	35.89	39.56	39.00	34.26	33.96	41.69	43.08	36.79	36.86	35.19
Total (calc.)	95.80	95.35	96.64	95.91	94.15	99.29	97.99	97.35	98.49	98.25	98.45	100.30	99.80	98.38
Si (apfu)	0.025		0.015	0.029	1.610	0.011	0.013	0.015	0.010	0.000	0.014	0.023	0.020	0.027
Ti	4.881	5.604	5.329	5.259	3.661	3.905	3.938	2.693	2.628	4.291	4.359	2.675	2.684	2.365
Al	2.308	0.965	0.689	0.655	0.314	0.529	0.452	0.381	0.391	0.659	0.388	0.538	0.809	0.495
Cr	0.000	0.000	0.000	0.000	0.000	0.006	0.003	0.005	0.000	0.000	0.005	0.013	0.020	0.008
Fe^{3+}	3.881	3.829	4.624	4.769	5.145	7.576	7.589	10.145	10.296	6.759	6.862	10.053	9.762	10.713
Fe^{2+}	10.428	11.655	11.961	11.638	8.806	9.651	9.657	9.207	9.109	10.460	10.921	9.180	9.163	8.974
Mn	0.130	0.173	0.195	0.165	0.219	0.377	0.416	0.864	0.865	0.506	0.599	0.699	0.460	0.658
Mg	2.339	1.736	1.156	1.319	4.157	1.823	1.754	0.554	0.576	1.305	0.773	0.809	1.062	0.749
Ca	0.008	0.038	0.031	0.166	0.071	0.033	0.082	0.015	0.001	0.020	0.075	0.011	0.019	0.006
Usp (%)	64.42	71.47	67.77	67.01	66.32	49.56	49.92	34.16	33.27	54.38	55.11	43.64	64.98	41.12

vi) Feldspar

The basanite and benmoreites contain plagioclase (Table 6) with compositions ranging respectively from labradorite ($An_{58}Ab_{33}$) to andesine ($An_{30-46}Ab_{59-49}$ and oligoclase ($An_{29}Ab_{59}$). In the benmoreites and trachyte, sanidine ($Or_{39-90}Ab_{55-10}$) and anorthoclase ($Or_{10-27}Ab_{62-59}$) were analyzed. BaO amounts in some crystals from benmoreite are < 1 wt.% (0.1−0.8 wt.%).

Table 6. *Representative chemical compositions and structural formula (on the basis of 8 oxygens) of feldspar (ph: phenocryst; m: microlite).*

lava-types	plagioclase							K-feldspar						
	basanite benmoreites							benmoreites					trachytes	
sample nb.	**127**	**207**	**207**	**207**	**207**	**207**	**207**	**207**	**207**	**207**	**207**	**207**	**293**	**293**
description	**ph**	**ph**	**ph**	**ph**	**ph**	**ph**	**ph**	**m**	**ph**	**ph**	**ph**	**m**	**ph**	**ph**
SiO_2 (wt.%)	50.93	56.96	58.26	58.80	58.22	61.00	60.87	64.64	66.37	65.08	65.37	64.34	64.45	63.94
Al_2O_3	29.74	25.78	26.58	25.50	26.78	24.76	24.19	18.70	19.60	19.27	19.97	21.16	20.34	20.36
FeO	0.93	0.37	0.47	0.45	0.34	0.29	0.36	0.02	0.30	0.30	0.38	0.34	0.23	0.27
CaO	12.61	8.88	8.74	6.96	8.90	6.13	5.69	0.00	0.79	0.67	0.95	1.83	0.81	0.87
Na_2O	3.96	5.61	5.37	6.59	5.57	6.83	6.68	1.09	6.52	5.42	6.06	7.10	5.38	5.30
K_2O	1.33	0.64	0.71	1.10	0.73	1.52	1.68	14.80	7.08	7.75	6.54	4.76	7.92	8.04
BaO		0.35	0.12	0.35	0.35	0.35	0.39	0.84	0.10					
Total	99.60	98.59	100.34	99.76	100.89	100.88	99.86	100.09	100.77	98.55	99.26	99.53	99.15	98.82
Si (apfu)	2.339	2.599	2.603	2.646	2.593	2.706	2.726	2.986	2.958	2.967	2.947	2.887	2.926	2.917
Al	1.610	1.386	1.400	1.352	1.406	1.294	1.277	1.018	1.029	1.036	1.061	1.119	1.088	1.095
Fe^{2+}	0.000	0.014	0.018	0.017	0.013	0.011	0.013	0.001	0.000	0.011	0.014	0.013	0.009	0.010
Ca	0.620	0.434	0.418	0.336	0.425	0.291	0.273	0.000	0.038	0.032	0.046	0.088	0.039	0.043
Na	0.353	0.498	0.467	0.577	0.483	0.589	0.582	0.098	0.565	0.481	0.531	0.619	0.475	0.470
K	0.078	0.037	0.041	0.063	0.041	0.086	0.096	0.872	0.402	0.451	0.376	0.273	0.459	0.468
Ba		0.006	0.002	0.006	0.006	0.006	0.007	0.015	0.002					
An (mol. %)	58.98	45.28	46.00	35.28	45.21	30.71	29.51	0.09	3.75	4.73	6.21	10.15	4.97	5.48
Ab	33.60	50.33	49.49	57.76	49.88	59.91	59.90	9.95	56.13	49.17	54.90	62.38	48.34	47.38
Or	7.42	4.39	4.51	6.96	4.90	9.38	10.59	89.96	40.12	46.10	38.89	27.47	46.68	47.14

vii) Apatite

Apatite crystal (Table 7) had been analyzed in benmoreites with P_2O_5 contents 42.6 wt.%. The amounts of F ranging between 2.9 wt.% and 7.2 wt.% (fluoro-apatite), and Cl contents are low (0.13−0.32wt.%).

Table 7. *Representative chemical compositions and structural formula (on the basis of 26 oxygens) of apatite (ph: phenocryst; m: microlite).*

lava-types	**benmoreites**						
sample nb.	**207**	**207**	**207**	**207**	**206**	**206**	**206**
description	**ph**	**ph**	**ph**	**ph**	**ph**		**ph**
SiO_2	0.36	0.31	0.27	0.25	0.42	0.38	0.38
La_2O_3					0.06	0.01	
Ce_2O_3					0.41	0.40	
FeO	0.28	0.18	0.27	0.28	0.08	0.00	0.59
CaO	51.98	52.88	53.33	52.96	53.44	53.60	54.71
P_2O_5	42.60	42.35	42.60	41.47	41.11	40.84	36.47
F	4.55	4.22	2.91	4.05	1.13	0.59	7.22
Cl	0.29	0.32	0.27	0.31			0.13
H_2O*	0.06	0.06	0.06	0.06	0.06	0.06	0.06
F as O	1.92	1.78	1.22	1.70	0.48	0.25	3.04
Cl as O	0.06	0.07	0.06	0.07			0.03
Total	100.12	100.32	99.71	99.38	97.19	96.12	100.08
Si (apfu)	0.057	0.050	0.045	0.040	0.073	0.068	0.061
La	0.000	0.000	0.000	0.000	0.002	0.000	0.000
Ce	0.000	0.000	0.000	0.000	0.013	0.013	0.000
Fe	0.037	0.024	0.037	0.038	0.011	0.000	0.080
Ca	8.841	9.154	9.418	9.304	9.994	10.165	9.486
P	5.858	5.793	5.945	5.757	6.075	6.119	4.995
F	2.285	2.154	1.515	2.099	0.624	0.330	3.695
Cl	0.077	0.087	0.076	0.087	0.000	0.000	0.034

viii) Amphibole

All analyzed crystals (Table 8) have Ti abundances higher than 0.5 apfu and are classified as kaersutite (Ti > 0.5) after [26]. In basanite (Figure 7) these crystals have ~ 14.1 wt.% of MgO. The Ti amount (~ 0.68 apfu) is lower than those of the kaersutite of the basalts from Tchabal Nganha (Ti: ~ 0.78 apfu; [1]). In benmoreites, the compositions of kaersutite megacrysts (mg#: ~ 0.67) and phenocrysts (mg#: ~ 0.66) are relatively similar. The Ti and Al^{iv} amounts for megacrysts (Ti: ~ 0.71 apfu; Al^{iv}: ~ 2.23 apfu) and phenocrysts (Ti: ~ 0.70 apfu; Al^{iv}: ~ 2.08 apfu) are similar. In the kaersutite megacryst, Sr contents 1900 ppm (See Table 10). Kaersutite from trachyte have the contents of Ti and Al^{IV} similar to those analyzed in basanite and benmoreites, apart from the F amounts (~ 1.18 wt.%) which are slightly more concentrated. Based on petrographic and geochemical observations, the studied amphiboles show no zonation and slight difference in major element composition. The REE elements analyzed on one amphibole megacryst sample from benmoreite show a general convex-upward REE pattern (see Figure 10 below) with LREE enrichment relative to HREE and maximum enrichment for Nd. The primitive mantle [27] normalized multi-element patterns for this amphibole differ considerably from the host rocks (see Figure 11 below) and are characterized by the strongly negative P, Zr anomalies and positive Sr, Ba anomalies with the value of Zr/Nb ratio below 3.

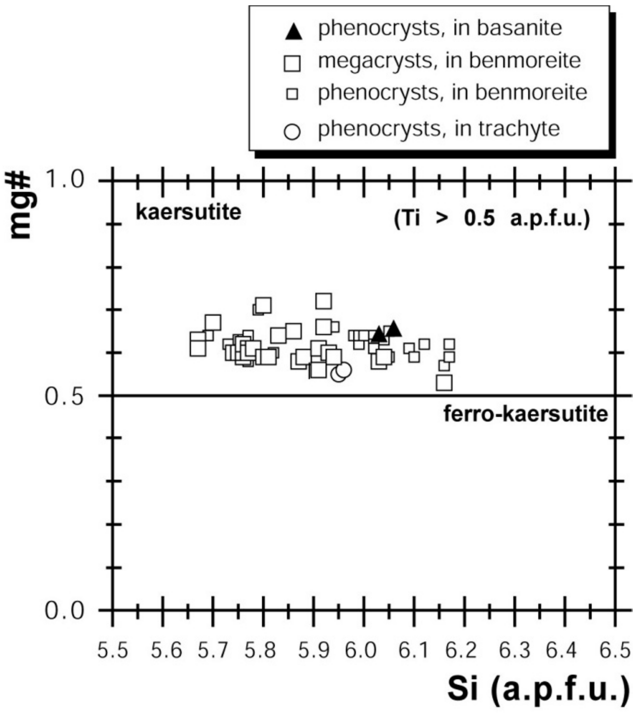

Figure 7. *Distribution of amphibole compositions analyzed in basalt, benmoreite and trachyte (according to the classification of [26]).*

Table 8. *Representative chemical compositions and structural formula (on the basis of 23 oxygens and 15 cations) of amphibole (megac: megacryst; ph: phenocryst; m: microlite).*

lava-types	basanite		benmoreite										trachyte	
sample nb.	127	127	207	207	207	207	207	207	207	207	206	206	293	293
description	ph		megac	megac	megac	ph	ph	megac	megac	megac	megac	megac	ph	ph
SiO_2 (wt.%)	40.69	41.03	38.26	38.37	38.92	40.49	39.32	39.36	38.32	37.90	39.35	40.27	39.01	39.09
TiO_2	6.15	5.40	6.01	6.17	6.19	4.63	6.24	6.27	5.95	5.85	5.37	5.35	5.43	5.14
Al_2O_3	12.43	12.71	14.85	14.28	14.36	11.75	12.44	12.98	14.29	14.34	12.59	12.30	11.85	12.25
FeO	8.20	8.07	12.30	11.94	12.22	13.69	10.94	11.81	12.08	11.77	12.83	13.37	14.13	13.31
MnO	0.06	0.11	0.16	0.18	0.19	0.62	0.18	0.25	0.00	0.10	0.26	0.11	0.56	0.47
MgO	13.95	14.15	11.08	11.06	11.30	10.50	12.31	11.30	11.15	11.03	11.62	11.26	10.69	10.95
CaO	12.98	13.04	10.91	11.94	11.91	10.83	11.07	11.29	11.68	11.52	11.54	11.34	11.53	11.67
Na_2O	2.58	2.60	2.31	2.60	2.42	2.53	2.77	2.49	2.63	2.61	2.66	2.70	2.83	2.76
K_2O	1.22	1.27	1.03	1.10	1.05	1.55	1.23	1.17	1.16	1.10	1.42	1.51	1.57	1.58
F	0.14	0.91	0.42	0.29	0.14	0.91	0.00	0.21	0.30	0.00	0.24	0.32	1.18	0.33
Cl	0.04	0.07	0.00	0.00	0.04	0.07	0.04	0.03	0.04	0.03	0.02	0.00	0.03	0.04
F as O	0.06	0.38	0.18	0.12	0.06	0.38	0.00	0.09	0.12	0.00	0.10	0.13	0.50	0.14
Cl as O	0.01	0.02	0.00	0.00	0.01	0.02	0.01	0.01	0.01	0.01	0.00	0.00	0.01	0.01
Total-(F+Cl)	98.34	98.78	97.08	97.76	98.63	96.98	96.52	97.01	97.39	96.21	97.75	98.34	98.09	97.35
FeO (calc)	8.20	8.07	10.21	11.94	12.22	13.69	10.94	11.81	12.08	11.77	12.83	13.37	14.13	15.82
Fe_2O_3 (calc)			2.69											
Si (apfu)	6.032	6.061	5.703	5.763	5.767	6.157	5.920	5.928	5.769	5.758	5.914	6.027	5.947	5.961
Ti	0.686	0.600	0.674	0.697	0.690	0.529	0.707	0.711	0.674	0.668	0.606	0.602	0.622	0.590
Al^{IV}	1.968	1.939	2.297	2.237	2.233	1.843	2.080	2.072	2.231	2.242	2.086	1.973	2.053	2.039
Al^{VI}	0.205	0.274	0.312	0.292	0.276	0.263	0.127	0.232	0.304	0.326	0.144	0.198	0.075	0.163
Fe^{3+}			0.294											
Fe^{2+}	1.722	1.643	1.239	1.756	1.612	1.793	1.453	1.665	1.697	1.646	1.648	1.812	1.975	1.937
Mn	0.008	0.014	0.020	0.023	0.023	0.080	0.023	0.032	0.000	0.012	0.033	0.013	0.072	0.061
Mg	3.084	3.116	2.462	2.476	2.496	2.381	2.763	2.537	2.503	2.498	2.604	2.512	2.429	2.489
Ca	2.061	2.064	1.742	1.921	1.891	1.765	1.785	1.822	1.883	1.875	1.858	1.818	1.883	1.907
Na	0.743	0.745	0.666	0.758	0.694	0.744	0.810	0.727	0.767	0.768	0.776	0.784	0.835	0.816
K	0.227	0.236	0.196	0.210	0.198	0.301	0.236	0.223	0.223	0.212	0.272	0.287	0.304	0.305
mg#	0.64	0.65	0.67	0.59	0.61	0.57	0.66	0.60	0.60	0.60	0.61	0.58	0.55	0.56

ix) Titanite

The titanite crystals (Table 9) with TiO_2 (~ 37.9 wt.%) and CaO (26.4–27.8 wt.%) contents were analyzed in trachyte.

Table 9. *Representative chemical compositions and structural formula (on the basis of 20 oxygens) of titanite (mph: microphenocryst).*

lava-type		trachyte	
sample nb.	293	293	293
description	mph		
SiO_2 (wt. %)	30.44	30.53	30.77
TiO_2	37.57	37.92	36.06
ZrO_2	0.00	0.00	0.00
La_2O_3	0.00	0.00	0.00
Ce_2O_3	0.00	0.00	0.00
Nd_2O_3	0.00	0.00	0.00
Y_2O_3	0.00	0.00	0.00
Al_2O_3	1.02	0.90	1.25
FeO	1.78	1.66	2.17
CaO	26.87	26.47	27.84
Na_2O	0.11	0.06	0.09
Fe_2O_3 (calc)	1.98	1.85	2.41
Total	97.99	97.74	98.41
Si (apfu)	4.096	4.107	4.142
Ti	3.802	3.836	3.650
Zr	0.000	0.000	0.000
Y	0.000	0.000	0.000
La	0.000	0.000	0.000
Ce	0.000	0.000	0.000
Nd	0.000	0.000	0.000
Al	0.081	0.072	0.099
Fe^{2+}	0.200	0.187	0.244
Fe^{3+}	0.000	0.000	0.000
Ca	3.874	3.815	4.016
Na	0.014	0.008	0.012

4.2.2. Whole Rock Chemistry

Nomenclature: The studied basaltic lava is a basanite, as classified with the TAS diagram (Figure 8; [28], [29]). In the same diagram, the felsic lava falls in the field of trachyte and the intermediate rocks are latites (Na_2O-2 < K_2O) with SiO_2 contents located between 53 wt.% and 57 wt. % (Table 10). According to this TAS diagram, latite is intermediate between shoshonite and trachyte. However, shoshonitic and potassic rocks are probably derived from anomalous mantle sources which were enriched in incompatible elements by subduction-related processes [30]. The studied intermediate rocks are sampled in an intraplate alkaline setting. From this consideration, the term benmoreite was appropriated according to the [31] diagram (see Figure 8). The high concentration of K_2O in these benmoreites could be linked to the accumulation of K-feldspar, mica and kaersutite

megacrysts or others processes as described below.

Table 10. *Whole-rock composition of studied lavas and kaersutite megacryst.*

lava-types	**basanite**	**benmoreites**		**kaersutite**	**trachyte**
sample nb.	**127**	**206**	**207**	**207Hb**	**293**
SiO_2 (wt %)	40.75	54.90	54.54	38.08	58.94
TiO_2	4.42	1.44	1.41	5.87	0.75
Al_2O_3	12.25	18.26	18.06	14.80	18.75
Fe_2O_3*	13.86	5.92	6.01	13.17	3.32
MnO	0.17	0.19	0.19	0.16	0.17
MgO	10.23	1.84	1.86	11.21	0.59
CaO	11.69	4.43	4.62	11.64	1.81
Na_2O	2.85	5.20	5.26	2.45	6.33
K_2O	1.34	4.51	4.69	1.11	6.19
P_2O_5	0.54	0.50	0.51	0.14	0.15
L.O.I	0.97	2.18	2.26	0.43	2.56
Total	99.08	99.37	99.41	99.01	99.56
D.I.	23.23	70.10	70.12		87.03
P.I.	0.50	0.74	0.76		0.91
Mg#	0.74	0.56	0.56		0.41
Be (ppm)	1.2	2.2	1.6	0.9	2.9
Rb	20	94	87	11	146
Sr	651	1426	1301	1904	441
Ba	378	1643	1578	904	1444
V	365	36	56	240	30
Cr	327	12	16	14	5
Co	59	7	6	26	5
Ni	118	14	17	19	5
Cu	51	12	12	61	5
Zn	122	109	101	86	101
Y	24.2	35.8	34.1	33.0	27.8
Zr	246	402	358	94	617
Nb	55	116	110	40	140
Hf	6.1				
Ta	4.42				
Th	3.66	8.51	13.00	6.00	14.00
U	1.1				
Pb	12.7		5.8		
Ga	20.99	23.10	23.00	16.00	24.00
La	36.0	100.6	96.8	11.2	116.9
Ce	80	202	181	41	209
Pr	10.1	22.7			
Nd	43.4	85.3	79.7	41.2	67.1
Sm	8.9	15.7	14.2	11.9	10.8
Eu	2.85	4.67	4.62	4.39	2.73
Gd	7.5	9.8	10.8	9.3	7.6
Tb	1.04				
Dy	5.4	7.5	6.9	7.0	5.3
Ho	0.9				
Er	2.2	3.3	2.9	2.6	2.6
Tm	0.3				
Yb	1.7	2.6	2.5	1.6	2.4
Lu	0.25	0.35	0.41	0.21	0.40
Zr/Nb	4.47	3.37	3.25	2.35	4.41
$(^{87}Sr/^{86}Sr)_{10Ma}$			0.7037		

Fe_2O_3*: total Fe as Fe^{3+}; L.O.I.: Loss on ignition; D.I.: Differentiation index (D.I.: = ∑Qtz+Or+Ab+Ne+Lc, CIPW norm); P.I.: Peralkaline index (P.I. = molar $[Na_2O + K_2O]/Al_2O_3$)

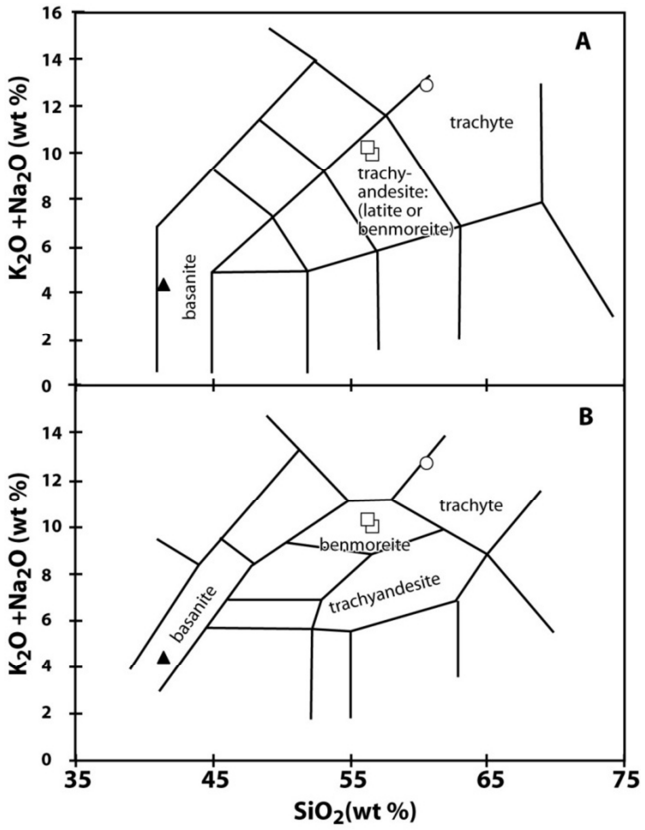

Figure 8. *Compositions of studied rocks in Total alkali–silica (TAS) diagram (A) ([28]) and (B) ([31]).*

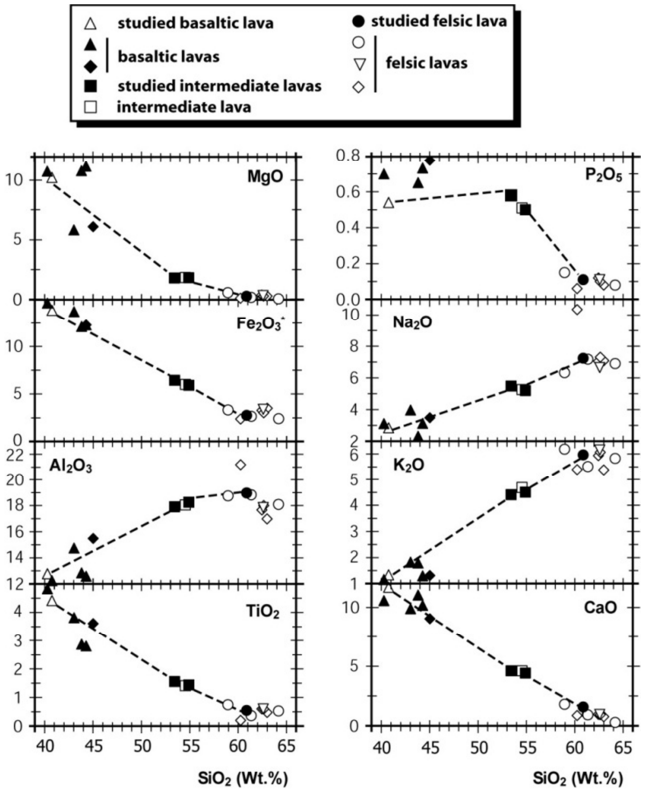

Figure 9. *Harker diagram for major elements of the studied rocks (the others data used are from the same sector [3].*

Major elements: The contents of Sr and Ba increase from basaltic lavas to the intermediate lavas and then fell sharply in felsic lava. In the major elements Harker diagram (Figure 9) several data from the previous Djinga Tadorgal study [3] are used for comparison and to establish the compositional trend. Overall, the compositional trend is similar. The amounts of TiO_2, Fe_2O_3*, MgO, CaO and P_2O_5 decrease with increasing SiO_2 contents. While Al_2O_3, K_2O and Na_2O increase with differentiation.

Trace elements: The contents of Sr and Ba exceed respectively 1300 ppm and 1500 ppm in benmoreites. Differentiated lavas such as benmoreites and trachyte from Djinga Tadogal are poor in transition elements (V, Cr, Co, Ni, Cu). These elements are more concentrated in basanite (Table 10). The values of Zr/Nb ratios are similar in basanite (4.47) and trachyte (4.41); but just below 4 (Zr/Nb: 3.25–3.37) in benmoreites. The primitive mantle [27] normalized REE patterns for the studied rocks are subparallel (Figure 10). The normalized REE pattern for trachyte displays a spoon-shape feature. The primitive mantle normalized multi-element patterns show for basanite, moderated negative K and P anomalies. Benmoreites display negative P, Ti and Rb anomalies. For trachyte, negative P, Sr and Ti anomalies are presented (Figure 11). One isotopic analysis ($(^{87}Sr/^{86}Sr)_{10Ma}$ = 0.7037) was performed for the studied benmoreite (sample 207).

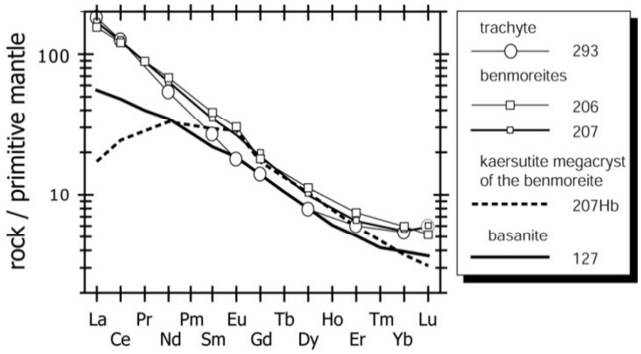

Figure 10. *Representative primitive mantle-normalized [27] REE patterns for basalt, benmoreite, trachyte and kaersutite megacryst from the Tignere volcanic domain.*

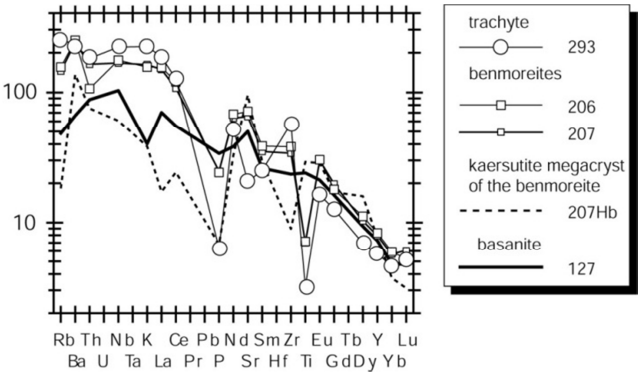

Figure 11. *Representative primitive mantle-normalized [27] multi-element patterns for basalt, benmoreite, trachyte and kaersutite megacryst from the Tignere volcanic domain.*

5. Discussion

5.1. Evidence of Cogenetic Origin and Inferences Concerning Crystallization

It is crucial to establish that the rocks selected for this study are related to each other by a genetic process that can be defined and tested explicitly. Thus, according to their coexistence in the same massif; their similar Zr/Nb ratios (~ 4.4) and their subparallel primitive mantle-normalized REE patterns, the basaltic and trachytic magmas from Tignere volcanic domain were derived from the same source.

For benmoreite, the value of Zr/Nb ratios is low (~ 3.3), whereas these rocks occurred in the same environment. However, the trace elements variations such as subparallel primitive mantle-normalized REE and the linear trends in the Harker diagram (oxides-oxides distribution; see Figure 9) could be used to justify the cogenetic origin of the studied rocks. The value of the isotopic $^{87}Sr/^{86}Sr$ ratio (0.7037) recalculated for 10 Ma for benmoreite, involves the absence of the significant crustal contamination.

Hydrothermal fluids can react with pre-existing minerals to generate others, as evidenced in basaltic lavas with the destabilization of amphibole into Fe-Ti oxides and rhönite [3]. In upper mantle-derived rocks, hydrous minerals (such as amphibole) give Information on the nature of the metasomatic event(s) [32].

5.2. Kaersutite Megacrysts Origin

The studied kaersutite megacrysts hosted in the benmoreite may represent (1) products of interaction of the magma with peridotitic wall rocks, (2) residual minerals from the ambient mantle, (3) igneous minerals that crystallized directly from the alkaline melt [33].

Two different types of amphibole (disseminated and vein amphibole) are described in mantle environments [34] and references therein). Disseminated amphibole from peridotite is typically in textural equilibrium with the host peridotite. The second type of amphibole is associated with metasomatic veins in mantle rocks. This amphibole was formed during an episode of modal metasomatism [35] caused by migration of subduction-related aqueous fluids from a shallow continental lithospheric mantle [36]. The primitive mantle-normalized REE pattern for the studied kaersutite megacrysts falls in the vein amphibole field (Figure 12). The majority of amphibole is optically homogeneous and unzoned with the absence of significant chemical zoning in kaersutite megacrysts and phenocrysts. These are typical for crystallization under similar physicochemical conditions. According to [34], hydrous veins with a solidus temperature lower than the ambient mantle will be the first to melt. This initial melting event will possibly generate hydrous phase-bearing mafic lavas [37] in which the hydrous phenocrysts may preserve the signature of the small metasomatic domains that yielded the alkaline melts. The kaersutite megacrysts are probably generated from a similar magma which has likely stagnated for a prolonged period in a H_2O-rich magmatic chamber. Temperature, pressure and fO_2 would have remained constant during this period [38].

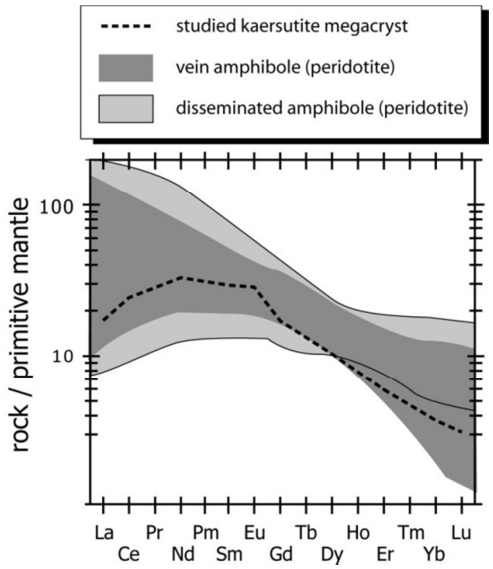

Figure 12. *Primitive mantle-normalized (McDonough and Sun 1995) REE patterns for the studied kaersutite megacryst; dark grey field represents vein amphibole and bright grey field peridotite amphibole ([36]; [34]).*

5.3. Modeling the Fractional Crystallization (FC), Assimilation and Fractional Crystallization (AFC), and Mixing Processes

Petrological processes, such as fractional crystallization (FC), combined fractional crystallization and assimilation (AFC), and mixing processes, which modify the geochemical composition of the magma, are graphically programmed on the basis of differentiation equations (see [39] for details). Only Rayleigh fractionation is considered. During the AFC process there is a strict relationship between the amount of material assimilated and the amount of material crystallized during cooling of the magma. The program enables the user to export outputs of linear- or logarithmic-scaled bivariate diagrams and also rare earth elements (REE) and multi-element spider diagrams of the modeling results. The sample 127 (basanite) is used as the starting composition (C_0) and the daughter is the benmoreite. The assimilant (C_a) selected is the upper continental crust [40].

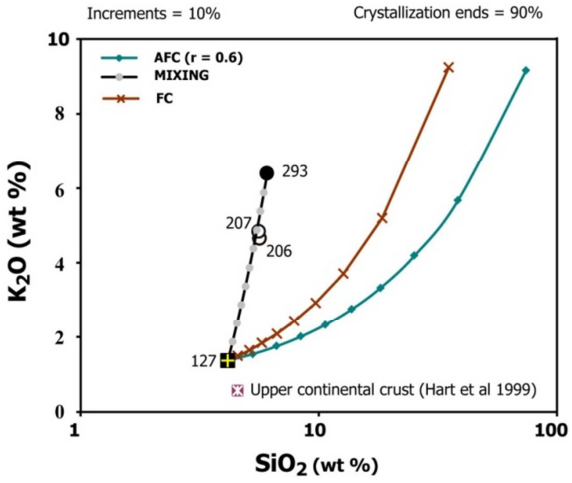

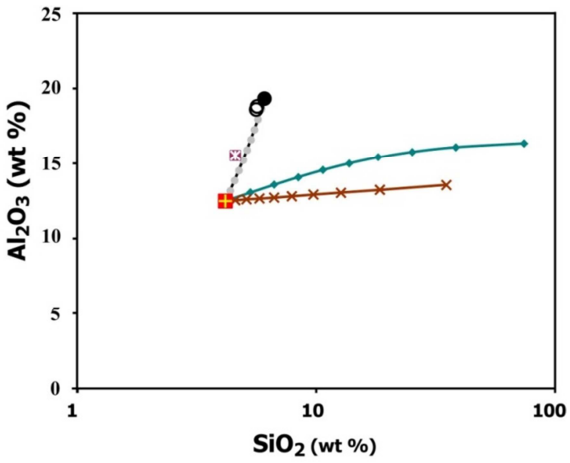

Figure 13. Effects of AFC, FC and mixing processes on the concentrations of major elements (Al_2O_3 and K_2O vs SiO_2).

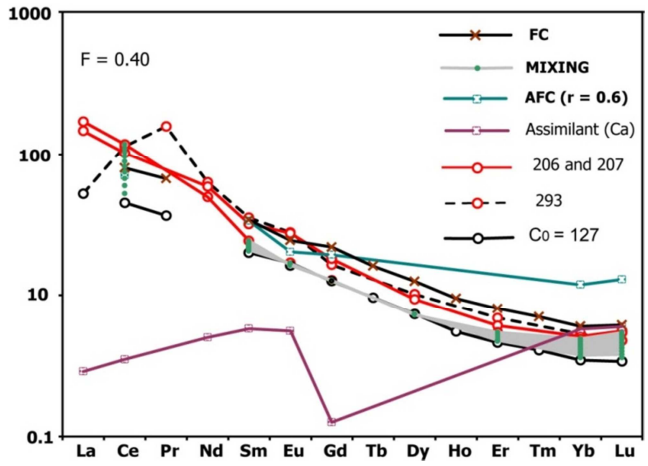

Figure 14. Modeling results of FC, AFC and mixing processes; REE-spider diagrams.

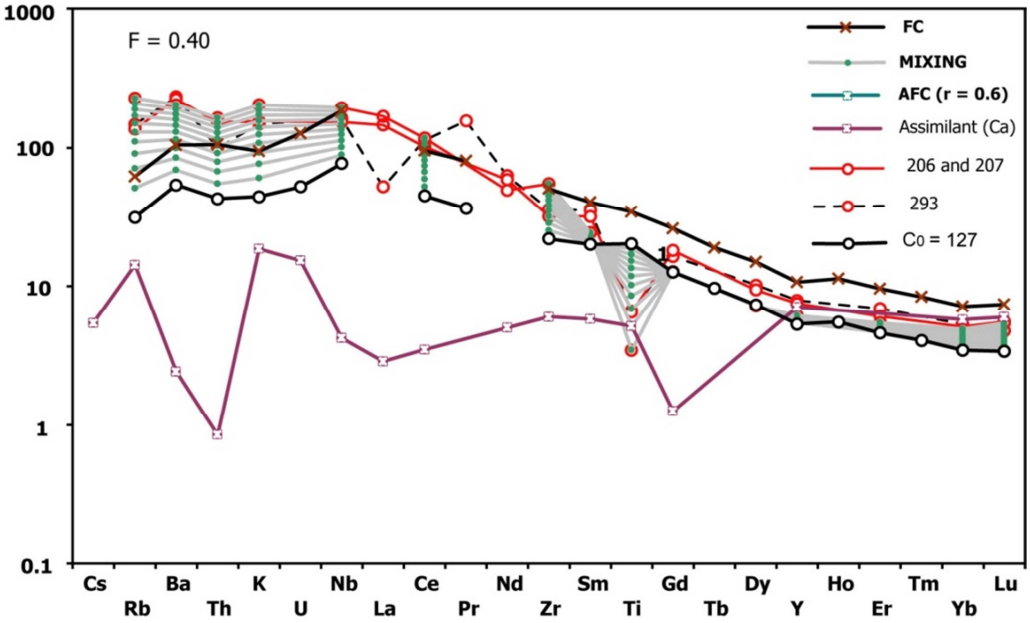

Figure 15. Modeling results of FC, AFC and mixing processes; multi-element-spider diagrams.

The theoretical curves for FC, AFC and mixing on figures 13, 14 and 15 have been calculated for F=0.40, the ratio of assimilated material to crystallized material is selected as r=0.6. The mixing process proposed is between basanite and trachyte. A magma mixing occurs when two separated magmas meet and the product is a single homogeneous or heterogeneous magma.

These modeling results are not very conclusive for mixing and AFC, but are acceptable for the FC process, as evidenced finally by the mass balance modeling for major elements (Table 11). The results are consistent with the fractional crystallization from basaltic lava to benmoreite (ol: 6.2; cpx: 18.6; pl: 22.3; ox: 12.3; $\sum r^2 = 0.18$).

The distribution of the analyzed mineralogical phases (phenocrysts) in the basaltic lava (data from [3]) is used for this modelling. Thus, for the studied domain it is possible to generate benmoreite by fractionation crystallization of basaltic melt. The least-square mass-balance values are low ($\sum r^2 = 0.18$) and acceptable for the evolutions from basaltic melt to benmoreite.

Table 11. Results of the mass balance modeling to generate benmoreites.

	basaltic lava measured	benmoreite measured					benmoreite calculated		
	120	207	ol	cpx	ox	plagio		Δ	Δ*Δ
Fractionation %			0.062	0.186	0.123	0.223			
SiO_2 (wt.%)	45.02	54.54	39.92	49.30	0.10	50.29	54.55	-0.01	0.00
TiO_2	3.61	1.41		1.33	22.9		1.34	0.07	0.00
Al_2O_3	15.48	18.06	0.01	5.97	2.70	29.89	18.01	0.05	0.00

	basaltic lava measured	benmoreite measured					benmoreite calculated		
	120	**207**	**ol**	**cpx**	**ox**	**plagio**		**Δ**	**Δ*Δ**
Fractionation %			**0.062**	**0.186**	**0.123**	**0.223**			
Fe_2O_3*	12.69	6.01	19.61	5.6	63.95	0.56	6.01	0.00	0.00
MnO	0.19	0.19	0.32	0.06	0.71		0.18	0.01	0.00
MgO	6.10	1.86	39.83	14.16	1.97		1.86	0.00	0.00
CaO	9.05	4.62	0.19	21.79		13.81	4.63	-0.01	0.00
Na_2O	3.49	5.26		0.39		5.90	5.15	0.11	0.01
K_2O	1.31	3.64					3.23	0.41	0.17
Total	96.94	95.59	99.88	98.60	92.33	100.45	94.95		
$\sum r^2$									0.18

Sample 120 ([3]); ol: olivine; cpx: clinopyroxene; ox: Fe-Ti oxide; plagio: plagioclase

6. Conclusions

The results of our study involve fractional crystallization processes. This fractional crystallization from basaltic melt to benmoreite are performed without significant crustal contamination ($(^{87}Sr/^{86}Sr)_{10Ma}$ = 0.7037). Hydrous minerals (such as amphibole) give Information on the nature of the metasomatic event(s) in upper mantle-derived rocks. Kaersutite megacrysts are likely generated during a long period in a H_2O-rich magmatic chamber under the constant temperature, pressure and fO_2 conditions.

Acknowledgements

Pr Bernard Déruelle is acknowledged for his assistance and his supervision during the laboratory-work at the university Pierre and Marie Curie (Paris VI).

References

[1] Nono A, Déruelle B, Demaiffe D, Kambou R (1994) Tchabal Nganha volcano in Adamawa (Cameroon): petrology of a continental alkaline lava series. J Volcano Geotherm Res 60: 147–178 doi: 10.1016/0377-0273(94) 90066-3.

[2] Nkouandou OF, Ngounouno I, Déruelle B, Ohnenstetter D, Montigny R Demaiffe D (2008) Petrology of the Mio-Pliocene volcanism to the North and East of Ngaoundéré (Adamawa, Cameroon). C R Geos 340: 28–37 doi: 10.1016/jcrte.2007.10.012.

[3] Mbowou GIB, Ngounouno I, Deruelle B (2010) Pétrologie du volcanisme bimodal du Djinga Tadorgal (Adamaoua, Cameroun). Rev. Cames. 11: 36–42.

[4] Macdonald R, Belkin HE, Fitton JG, Rogers NW, Nejbert K, Tindle AG, Marshall AS (2008) The roles of fractional crystallization, magma mixing, crystal mush remobilization and volatilemelt interactions in the genesis of young basalt peralkaline rhyolite suite, the Greater Olkaria Volcanic Complex, Kenya Rift Valley. J Petrol 49: 1515–1547 doi: 10.1093/petrology/egn036.

[5] Macdonald R (2012) Evolution of peralkaline silicic complexes: lessons from the extrusive rocks. Lithos 152: 11–22 doi: 10.1016/j.lithos.2012.01.014.

[6] Peretyazhkoa IS, Savinaa EA, Karmanovb NS, Shcherbakova Yu D (2015) Genesis of mugearites and benmoreites of Nemrut Volcano, Eastern Turkey: Magma mixing and fractional crystallization of trachybasaltic melt. Petrology 23: 376–403.

[7] Ngounouno I, Moreau C, Déruelle B, Demaiffe D, Montigny R (2001) Pétrologie du complexe alcalin sous-saturé de Kokoumi (nord du Cameroun). Bull Soc Géol France 172: 675–686.

[8] Lissom J (1991) Etude pétrologique des laves alcalines du massif d'Oku: un ensemble volcanique de la Ligne du Cameroun. Thèse de Doctorat. Université Pierre et Marie Curie, Paris 6. Pp 1–205.

[9] Clocchiatti R, Tanguy J (2002) Mégacristaux d'amphibole dans les laves de l'Etna (l'éruption de juillet-août 2001). 19ème Réunion des Sciences de la Terre, Nantes, France. Pp 1–94.

[10] Borley GD, Suddady P, Scott P (1971) Some xenoliths from the Alkalic Rocks of Tenerife, Canari islands. Contrib Mineral Petrol 31: 102–114 doi: 10.1007/bf00373453.

[11] Bédard JH (1988) Comparative amphibole chemistry of the Monteregian and Mountain alkaline suites, and the origin of amphibole megacrysts in alkali basalts and lamprophyres. Mineral Mag 52: 91–103.

[12] Toteu SF, Penaye J, Van Schmus WR, Michard A (1994) Preliminary U–Pb and Sm–Nd geochronologic data on the North-Central Cameroon: contribution of an Archean and paleo-Proterozoic crust to the edification of an active domain of the Pan-African orogeny. C R Acad Sci Paris 319: 1519–1524.

[13] Moreau C, Regnoult J-M, Déruelle B, Robineau B (1987) A new tectonic model for the Cameroon Line. Tectonophysics, 139: 317–334 doi: 10.1016/0040-1951(87)90206-x.

[14] Penaye J, Toteu SF, Tchameni R, Van Schmus WR, Tchakounté J, Ganwa A, Minyem D, Nsifa EN (2004) The 2.1 Ga West Central African Belt in Cameroon: extension and evolution. J Afr Earth Sci 39: 159–164 doi: 10.1016/j.jafrearsci.2004.07.053.

[15] Castaing C, Feybesse JL, Thiéblemont D, Triboulet C, Chèvremont P, (1994) Palaeogeographical reconstructions of the Pan-African/Brasiliano orogen: closure of an oceanic domain or intracontinental convergence between major blocks? Precambr Res 69: 327–344 doi: 10.1016/0301-9268(94)90095-7.

[16] Toteu SF, Van Schmus RW, Penaye J, Michard A (2001) New U–Pb and Sm–Nd data from north-central Cameroon and its bearing on the pre-Pan-African history of central Africa. Precam Res 108: 45–73 doi: 10.1016/s0301-9268(00)00149-2.

[17] Vicat JP, Ngounouno I, Pouclet A (2001) Existence de dykes doléritiques anciens à composition de tholéiites continentales au sein de la province alcaline de la ligne du Cameroun. Implication sur le contexte géodynamique. C R Acad Sci Paris 332: 243–249 doi: 10.1016/s1251-8050(01)01526-9.

[18] Pouchou JL, Pichoir F (1991) Quantitative analysis of homogeneous or stratified microvolumes applying the model «PAP». In: Electron Probe Quantification, K. F. J., Heinrich, D. E., Newbury (Eds) Plenum Press, New York, 31–75.

[19] Carignan J, Hild P, Mevelle G, Morel J, Yeghicheyan D (2001) Routine analyses, of trace elements in geological samples using flow injection and low pressure on liquid chromatography coupled to ICP-MS: a study of geochemical reference materials BR, DR-N, UB-N, AN-G and GH. Geostandards Newsletters 25: 187–198 doi: 10.1111/j.1751-908x.2001.tb00595.x.

[20] Roeder PL, Emslie RF (1970) Olivine-liquid equilibrium. Contrib Mineral Petrol 29: 275–289 doi: 10.1007/bf00371276.

[21] Morimoto A N and 8 co-authors (1988) Nomenclature of pyroxenes, IMA. Mineral Mag 52: 533–550.

[22] Wass SY (1979) Multiple origins of clinopyroxenes in alkali basaltic rocks. Lithos 12: 115–132 doi: 10.1016/0024-4937(79)90043-4.

[23] Avanzinelli R, Bindi L, Menchetti S, Conticelli S (2004) Crystallisation and genesis of peralkaline magmas from Pantelleria Volcano, Italy: an integrated petrological and crystal-chemical study. Lithos, 73: 41–69. doi: 10.1016/j.lithos.2003.10.007.

[24] Kunzmann T (1999) The ænigmatite-rhönite mineral group. Eur. J. Mineral. 11: 743–756.

[25] Deer WA., Howie Zussman J (1992). An Introduction to the rock-forming Minerals, 2nd ed, Pearson Prentice Hall, Harlow, 696pp.

[26] Leake BE, Wooley AR, Birch WD, Gilbert MC, Grice JD, Hawthorne FC, Kato A, Kisch HJ, Krivovichev VG, Linthout K, Laird J, Mandarino J (1997) Nomenclature of Amphibole: Repport of the Subcommitee on Amphiboles of the International Association Commission on New Minerals and Mineral Names. Mineral Mag 61: 295–321.

[27] McDonough WF, Sun SS (1995) The composition of the Earth. Chem Geol 120: 223–253 doi: 10.1016/0009-2541(94)00140-4.

[28] Le Bas, MJ, Le Maitre RW, Streckeisen A, Zanettin B (1986). A chemical classification of volcanic rocks based on the total alkali-silica diagram. J Petrol 27: 745–750. doi: 10.1093/petrology/27.3.745.

[29] Le Maitre RW (2002) Igneous rocks: a classification and glossary of terms: recommendations of the International Union of Geological Sciences, Sub- commission on the Systematics of Igneous Rocks. Cambridge University Press, Cambridge UK 236 pp.

[30] Ellam RM, Hawkesworth CJ, Menzies MA, Rogers NV (1989) The volcanism of southern Italy: role of subduction and the relationship between potassic and sodic alkaline magmatism. J geophys Res 9: 4589-4601 doi: 10.1029/jb094ib04p04589.

[31] Cox KG, Bell JD, Pankhurst RJ, (1979) In: The Interpretation of Igneous Rocks. George Allen & Unwin, London 450 pp.

[32] Powell W, Zhang M, O'Reilly SY, Tiepolo M (2004) Mantle amphibole trace-element and isotopic signatures trace multiple metasomatic episodes in lithospheric mantle, Western Victoria, Australia. Lithos 75: 141–171. doi: 10.1016/j.lithos.2003.12.017.

[33] Shaw CSJ, Eyzaguirre J (2000) Origin of megacrysts in the mafic alkaline lavas of West Eifel volcanic field, Germany. Lithos 50: 75-95 doi: 10.1016/s0024-4937(99)00048-1.

[34] Mayer B, Jung S, Romer RL, Pfänder JA, Klügel A, Pack A, Gröner E (2014) Amphibole in alkaline basalts from intraplate settings: implications for the petrogenesis of alkaline lavas from the metasomatised lithospheric mantle Contrib Mineral Petrol 167: 989–810 doi: 10.1007/s00410-014-0989-3.

[35] Witt-Eickschen G, Kaminsky W, Kramm U, Harte B (1998) The nature of young vein metasomatism in the lithosphere of the West Eifel (Germany): Geochemical and isotopic constraints from composite mantle xenoliths from the Meerfelder Maar. J Petrol 39: 155–185 doi: 10.1093/petroj/39.1.155.

[36] Witt-Eickschen G, Seck HA, Mezger K, Eggins SM, Altherr R (2003) Lithospheric mantle evolution beneath the Eifel (Germany): Constraints from Sr-Nd-Pb isotopes and trace element abundances in spinel peridotite and pyroxenite xenoliths. J Petrol 44: 1077–1095 doi: 10.1093/petrology/44.6.1077.

[37] Hawkesworth CJ, Gallagher K (1993) Mantle hotspots, plumes and regional tectonics as causes of intraplate magmatism. Terra Nova 5: 552–559 doi: 10.1111/j.1365-3121.1993.tb00304.x.

[38] Conner AB (2000) The mineral kaersutite and its occurrences. Senior Thesis, The Ohio State University. Pp 1–12.

[39] Ersoy Y, Helvacı C (2010) FC–AFC–FCA and mixing modeler: A Microsoft Excel spreadsheet program for modeling geochemical differentiation of magma by crystal fractionation, crustal assimilation and mixing. Computers & Geosciences 36: 383–390 doi: 10.1016/j.cageo.2009.06.007.

[40] Hart SR, Blusztajn J, Dick HJB, Meyer PS, Muehlenbachs K (1999) The fingerprint of seawater circulation in a 500-meter section of ocean crust gabbros. Geochimica et Cosmochimica Acta 63: 4059–4080 doi: 10.1016/s0016-7037(99)00309-9.